Development 133, 711-723 doi:10.1242/dev.02251

Developmental control of nuclear morphogenesis and anchoring by *charleston*, identified in a functional genomic screen of *Drosophila* cellularisation

Fanny Pilot[1], Jean-Marc Philippe[1], Céline Lemmers[1], Jean-Paul Chauvin[2] and Thomas Lecuit[1,*]

Morphogenesis of epithelial tissues relies on the precise developmental control of cell polarity and architecture. In the early *Drosophila* embryo, the primary epithelium forms during cellularisation, following a tightly controlled genetic programme where specific sets of genes are upregulated. Some of them, for example, control membrane invagination between the nuclei anchored at the apical surface of the syncytium. We used microarrays to describe the global programme of gene expression underlying cellularisation and identified distinct classes of upregulated genes during this process. Fifty-seven genes were then tested functionally by RNAi. We found six genes affecting various aspects of cellular architecture: membrane growth, organelle transport or organisation and junction assembly. We focus here on *charleston* (*char*), a new regulator of nuclear morphogenesis and of apical nuclear anchoring. In *char*-depleted embryos, the nuclei fail to maintain their elongated shape and, instead, become rounded. In addition, together with a disruption of the centrosome-nuclear envelope interaction, the nuclei lose their regular apical anchoring. These nuclear defects perturb the regular columnar organisation of epithelial cells in the embryo. Although microtubules are required for both nuclear morphogenesis and anchoring, *char* does not control microtubule organisation and association to the nuclear envelope. We show that Char is lipid anchored at the nuclear envelope by a farnesylation group, and localises at the inner nuclear membrane together with Lamin. Our data suggest that Char forms a scaffold that regulates nuclear architecture to constrain nuclei in tight columnar epithelial cells. The upregulation of Char during cellularisation and gastrulation reveals the existence of an as yet unknown developmental control of nuclear morphology and anchoring in embryonic epithelia.

KEY WORDS: Cellularisation, Nuclear envelope, Epithelial morphogenesis, *dappled*, RNAi, Microarrays, *Drosophila*

INTRODUCTION

The regulation of cell shape and cell polarity during development underlies the morphogenesis of tissues. In epithelia, tissues in which the cells exhibit an apicobasal polarity, both the cell surface, the organelles and cytoskeletal elements are precisely organised. Identifying the developmental pathways controlling cell shape at the cellular level is thus an important task for further our understanding of development.

As with most developing embryos, the first morphogenetic process in *Drosophila* embryos is the formation of the primary epithelium, a process called cellularisation (Foe et al., 1993; Schejter and Wieschaus, 1993b). Cellularisation is a specialised form of embryonic cleavage that yields a polarised epithelium within 1 hour (Lecuit, 2004). Upon egg laying, the newly fertilised embryo undergoes a series of 13 synchronous nuclear divisions in a syncytium, producing about 6000 nuclei at the cell cortex. During cellularisation, the plasma membrane invaginates in a slow phase and a fast phase between the nuclei, thus packaging each nucleus, other organelles and cytoskeletal elements into about 6000 cells (Lecuit and Wieschaus, 2000). Cellularisation involves the polarised growth of the plasma membrane via the vectorial transport of vesicles through the Golgi and recycling endosomes and their insertion at specific sites of the plasma membrane (Lecuit and Wieschaus, 2000; Papoulas et al., 2005; Pelissier et al., 2003; Sisson et al., 2000). Distinct plasma membrane domains are already established by this time. Polarised growth culminates in the formation of apical adherens junctions at the end of cellularisation and their subsequent stabilisation during gastrulation (Muller and Bossinger, 2003). Failure to form or stabilise apical junctions results in strong epithelial defects later on during gastrulation (Cox et al., 1996; Muller and Wieschaus, 1996; Tepass et al., 1996; Uemura et al., 1996). In addition, the formation of the primary epithelium involves the polarised organisation of the cytoskeleton and organelles. Microtubules (MTs) form an apicobasal network, with subpopulations of long MTs extending the plus ends basally around the nuclei and short MTs projecting towards the cortex. MTs control the apicobasal distribution of organelles, the nuclei being anchored apically, the Golgi apparatus mostly basal and lipid droplets undergoing basal and apical movements in two successive waves called clearing and clouding phases (Foe et al., 1993; Schejter and Wieschaus, 1993b; Sisson et al., 2000; Welte et al., 1998). The formation of the primary epithelium thus offers a good system with which to address how core cellular processes are developmentally regulated to produce a highly organised tissue exhibiting polarity at the cell surface and in the cytoplasm.

Cellularisation is concomitant with zygotic genome activation and inhibition of zygotic transcription totally blocks cellularisation (Foe et al., 1993). However, only five zygotic genes have been reported for their role in cellularisation: *nullo*, *Serendipity-α* (*Sry-α*) and *slam*, which are necessary for stabilisation of the membrane front called the furrow canal; *bottleneck* (*bnk*), which ensures the correct timing of basal closure of the cells; and *frühstart* (*frs*), required for the arrest in interphase 14 (Grosshans et al., 2003; Lecuit et al., 2002; Postner and Wieschaus, 1994; Rose and Wieschaus, 1992;

[1]Institut de Biologie du Développement de Marseille (IBDM) Laboratoire de Génétique et de Physiologie du Développement (LGPD), UMR6545 CNRS-Université de la Méditerrannée. Campus de Luminy case 907, Marseille 13288 cedex9, France. [2]Plateforme de microscopie électronique, IBDM, France.

*Author for correspondence (e-mail: lecuit@ibdm.univ-mrs.fr)

Accepted 14 December 2005

Schejter and Wieschaus, 1993a; Schweisguth et al., 1990; Stein et al., 2002). Remarkably, these five genes are strongly induced during cellularisation. The fact that the expression of *nullo*, *Sry-α*, *bnk*, *frs* and *slam* display a strong zygotic induction in cellularisation prompted us to screen for other genes induced during and required for cellularisation.

It has become a major challenge to integrate into a global cellular network, the distinct pathways underlying the numerous aspects of epithelial polarity. Functional genomic approaches based on RNA interference (RNAi), mostly in *Caenorhabditis elegans* embryos and *Drosophila* cells, have contributed to the identification of many genes involved in cellular organisation, based on their knock-down phenotype (Boutros et al., 2004; Fraser et al., 2000; Gonczy et al., 2000; Kamath et al., 2003; Kiger et al., 2003; Sonnichsen et al., 2005). The major advantage of such RNAi screens is the direct association of a gene to a given biological function. Novel approaches using expression profiling have also proven successful in identifying genes whose expression correlates with specific cellular processes (Arbeitman et al., 2002; Stathopoulos et al., 2002; White et al., 1999). Here, we have sought to combine such genomic methodologies and functional screens to extend the repertoire of genes involved in epithelial architecture. The screen was performed in early *Drosophila* embryos. Instead of screening the full genome in a blind fashion, we have first established the repertoire of genes induced during *Drosophila* epithelial formation and subsequently tested their role by RNAi in early embryos. We could thus test a selected and limited group of genes making it possible to assess their function more thoroughly using time-lapse recordings.

This screen uncovered new genes required for various aspects of cellularisation. One of them, *charleston* (*char*), on which we focus most of this study, controls nuclear morphogenesis in epithelial cells. In *char*-depleted embryos, lateral constraints that elongate the nuclei along the apicobasal axis are disrupted and the nuclei round up. In addition, the nuclei lose their apical anchoring. Together, these nuclear defects distort the regular columnar organisation of epithelial cells in the gastrula. Char localises at the nuclear envelope via a lipid anchor and plays a structural role in nuclear morphogenesis.

MATERIALS AND METHODS

Fly strains

OreR and *yw* flies were used as wild-type strains. The following stocks were used: *Df(3R)C4,p*/Dp(3;3)P5,Sb1* generates a deletion at the *char* locus and is referred to as *Dfchar*. We also used *Df(3R)5780/TM2* (Exelexis, P{w[+mW.Scer\FRT.hS4]=3′.RS6+3.3′}ED5780/TM2) to generate transheterozygous combinations with *yw*; *P{EPgy2}CG5175[EY07696]*, a viable *char* mutant referred to as $char^{EY07696}$ in the Results section. The other mutant strain used is $Lac^{BG01462}$. UAS-HAChar, UAS-HACharΔCSIM and UAS-dpld ($dpld^{EP1050}$ and $dpld^{EP2291}$ EP lines) males were crossed to *mat(Tub-Gal4VP16 (67c); mat(Tub-Gal4VP16 (15) (67;15)* females and raised at 18°C. A ru^{1} $klarsicht^{1}$ fly stock (gift from M. Welte) was used for injected embryos shown in Fig. S4 (see supplementary material) to reveal the gastrulation defects better.

Constructs

UAS-HA-Char

A HA3-CG5175 chimera cDNA (N-terminal HA tag in 3 copies, inserted in frame after the second AUG of CG5175) was generated by PCR (positions 158-1870 of the cDNA AY094778 in GenBank). The PCR fragment digested by *Eco*RI was inserted into pUAS-T generating pUAS-T-HA-Char.

UAS-HA-CharΔCSIM

We mutagenised the pUAS-T-HA-Char vector to introduce a TGA stop codon in place of the TGC (cystidine at amino acid C567). This modification results in the deletion of the last four (CSIM) C-terminal amino acids. All constructs were sequenced.

Microarray experiments

Thirty minute egg collections of *OreR* and *yw* flies at 25°C were aged at room temperature (RT) according to the different temporal classes T0-T4. Embryos were dechorionated with 50% bleach, put on a cover slip and covered with Halocarbon oil 27 (Sigma). Embryos of the appropriate stage were manually selected under the dissecting scope. Selected embryos were transferred to a basket, rinsed with PBS with 0.7% NaCl, 0.04% triton-X100 and placed on ice in the Trizol solution (GibcoBRL). Trizol extraction of total RNA was performed according to the manufacturer's instructions. The quantification was assessed by OD, and the quality on agarose gel. Three independent pools of 25 μg of total RNA, for each time-point, were sent to Affymetrix (Illkirch, FRANCE) for hybridisation on Release 2 microarrays. Microarray data analysis was performed with Windows Excel and TreeView and Cluster (Eisen laboratory) softwares.

Clustering was performed using hierarchical clustering with average linkage using the Cluster software (information available upon request: pilot@ibdm.univ-mrs.fr). For the clusters shown in Fig. 1B-D, a list of genes with potential high variations of expression was first selected from Table S1A (see supplementary material) using the following criteria: at least three present (P) assignments among the 15 values (three independent experiments for each of the five time points); a maximal value among the 15 values of more than 200; and a standard deviation of more than 100 among the 15 values.

dsRNA synthesis

The 500 bp PCR products of the selected genes were from the 'Heidelberg GenomeRNAi *Drosophila* resources'.

A second probe for *dappled* was made by PCR amplification of genomic DNA (nucleotides 1978 to 2665 of the transcript AY060421, GenBank) with the following pair of primers containing the sequence of the T7 promoter (TAATACGACTCACTATAGGGAGACCAC): *dpld*-T7-F, T7seq GCTCTTGATTGGGAACTCAATGG; and *dpld*-T7-R, T7seq CGTTGATGTCTGGATCAATCAGG.

A second probe targeted against the 3′UTR of *char* was made by PCR amplification of genomic DNA (between positions +5 to +366, 3′ of the stop codon) with the following set of primers: *char3′UTR*-T7-F, T7seq CAGGCCAGACCACATAATACC; and char3′UTR-T7-R, T7seq GCGAAACAATACATGAACTCGGC.

Transcription from the T7 promoters was performed with Ambion MEGAscript or Promega Ribomax kits. dsRNA were resuspended in DEPC-treated water, quantified by OD, checked on agarose gel and diluted for RNAi at about 3-4 μM in DEPC-treated water.

RNAi screen

Embryos from 30 minute egg-collections of *OreR* and *yw* flies at 25°C were dechorionated in 50% bleach, aligned on agar, stuck on heptane-glued cover slips, dessicated and covered with Halocarbon 200 oil. Embryos were injected with dsRNA, stored at 25°C. Phase-contrast time-lapse images were collected on an inverted microscope (Zeiss) and a programmable motorised stage to record different positions over time (Mark&Find module from Zeiss). The system was run with AxioVision software (Zeiss). At least 40 timelapse movies from two independent injection series were performed for each dsRNA probe. Embryos were then let to develop at room temperature. Control embryos for RNAi were non-injected embryos [DIC control for *char*, *halo* and *btsz* in Fig. 3, Fig. S2 and Fig. S4 (see supplementary material)] or injected embryos with DEPC-treated water (all other cases).

RT-PCR

RNAi efficiency was estimated by measuring endogenous mRNA levels using RT-PCR after injection of dsRNA probe against *dpld*. Total RNA extraction from early gastrulating embryos, retro-transcription and PCR reactions were adapted from (Desbordes and Sanson, 2003). Primers used were *dpld-T7-F* and *dpld-T7-R* for *dpld* and *actin42-F* (ACTCCTACATATTTCCATAAA) and *actin42-R* (CTCCAGGGACGAGCTTGAA) for *Actin 42A*. PCR were performed on four sample dilutions for control and RNAi embryos (1:1; 1:3; 1:9; 1:27), with 30 amplification cycles. In these conditions, the amount of PCR products correlated to the cDNA input. cDNA contents between control and RNAi embryos were normalised to *actin 42A* PCR products. A threefold depletion of *dpld* cDNA was observed

in *dpld* RNAi embryos compared with control embryos. Similar experiments were performed for *btsz* RNAi. A fourfold depletion was observed for *btsz* in *btsz* RNAi embryos (F.P., J.-M.P., C.L. and T.L., unpublished). RT-PCR specific to the *CG5175/char-RA* and *CG5175/char-RB* transcripts was performed in early embryos using the following primers (see Fig. S4): CG5175-AF, AGGTCCCACTAGCGCGTTG; CG5175-BF, AAGCTTCA-GACTTGAATGTGTGC; and CG5175-CR, GGGAACTTCAGCTACC-ACCAC.

Farnesyl-transferase inhibitor experiments

Injections of FTI-277

Embryos were injected with FTI-277 at a final concentration of 10-20 μM [injection of 1 mM FTI-277 (Sigma) in early embryos (about 30 minutes old after egg laying)]. This produced a very penetrant (>95%) *char*-like phenotype. Injection shortly before cellularisation (during cycles 10-12) produced a milder and less penetrant phenotype. Embryos were then imaged for time-lapse recordings or fixed and stained as indicated for RNAi.

Cell culture experiments with FTI-277

S2 cells were cultured in Schneider's medium (Sigma) containing 10% FBS (foetal bovine serum) and maintained at 25°C. Cells were co-transfected with pUAS-T constructs and pMt-Gal4-VP16 vector using Fugene 6 (Roche) according to the manufacturer's instructions. Transfected cells were analysed after 24 hours of cDNA expression induced with 0.5 mM $CuSO_4$ and incubation with FTI-277 at different concentrations (10 to 40 μM). The cells were lysed 30 minutes at 4°C in NET buffer (50 mM Tris pH 7.5, 400 mM NaCl, 5 mM EDTA, 1% NP40 supplemented with anti-protease). The lysates were clarified by centrifugation and analysed by western blot after SDS-PAGE. Rat anti-HA (Roche) was used at a 1/2000 concentration and revealed by anti-rat HRP and Lumi-Light Western Blotting Substrate (Roche).

GST pull down

Transfected *Drosophila* S2 cells were washed in cold PBS and lysed in buffer A (1% NP-40, 50 mM Tris pH 7.5, 10 mM EDTA, 3 mM $MgCl_2$ supplemented with pepstatin, leupeptin and antipain 1 μg ml^{-1}, benzamidine 15 μg ml^{-1}, 1 mM sodium orthovanadate and 5 mM sodium pyrophosphate). The lysates were clarified by centrifugation, incubated with 50-70 μg of GST and GST fusion protein coated on Gluthatione Sepharose 4B beads (Amersham Biosciences) overnight at 4°C. After washes, the protein complexes were analysed by western blot after SDS-PAGE. Rat anti-HA (Roche) was used at a 1/2000 concentration.

Antibody production against Char

An antibody against the peptide EEVDVEEEQ was generated in rabbits (Eurogenetec). The serum was affinity purified against the peptide.

Immunofluorescent and chemofluorescent staining

Staining of non-injected embryos was carried out on overnight collections at 25°C. After dechorionation with bleach, embryos were fixed for 20 minutes in 4% formaldehyde (HA, Lamin, WGA and Char staining) and devitellinised by methanol popping. Injected embryos were prepared as described above and fixed during cellularisation. Embryos were fixed in 4% formaldehyde as described above (Lamin, PatJ and Bodipy staining) or in 17% formaldehyde (α- and γ-tubulin staining) or heat-fixed in 10 ml of boiling HF buffer (68 mM NaCl, 0.03% Triton X100) and rapidly cooled with ice and cold HF buffer (Neurotactin staining). In general, embryos were then rinsed with methanol and transferred in BBT (PBS, 0.1% Tween-20, 0.1% BSA, 0.01% NaN3). For Bodiby and phalloidin labelling, however, the embryos were directly transferred to BBT. Injected embryos were then hand-peeled in BBT. Antibody staining was performed in BBT (Neurotactin, Patj, α- and γ-tubulin) or in BBTx (PBS, 0,1% BSA, 0,1% Triton X-100) (HA, Lamin and Char) at the following concentrations: mouse Neurotactin BP106, 1/50 (Developmental Study of Hybridoma Bank, DSHB); guinea pig even-skipped, 1/100 (gift of J. Reinitz and D. Kosman); mouse α- and γ-tubulin, 1/200 (Sigma); mouse HA 12CA5, 1/200 (Roche); rabbit Char, 1/100; mouse Lamin ADL67.10, 1/200 (DSHB); rabbit PatJ (previously known as Dlt, gift of H. Bellen and M. Bhat), 1/300. Secondary antibodies were conjugated to Alexa488, Alexa546 and Cy5. Bodipy 505/515 (Molecular Probes) was used for lipid staining at 100 μM (from a DMSO stock at 10 mM) for 20 minutes. Nuclear staining was made with Hoechst 33258 (Sigma) at 0.2 μg/ml for 20 minutes and F-actin staining with TRITC-conjugated phalloidin (Sigma) at 1:500 for 20 minutes. All confocal images were obtained on a Zeiss LSM510 laser-scanning microscope using a 40× C-Apochromat water immersion objective (NA: 1,2) except for high resolution images in Fig. 9C-D′ where a 63× (NA: 1.4) oil immersion objective was used on a Leica SP2-NE confocal microsocope.

Immunofluorescence of S2 cells with triton or digitonin permeabilisation

S2 cells were fixed in 3% PFA for 25 minutes, and permeabilised with either 0.1% TritonX-100 for 10 minutes at room temperature, or 5 minutes with 40 μg/ml Digitonin in PBS at 4°C. After saturation with 0.2% gelatin in PBS for 30 minutes, S2 cells were incubated with primary antibodies following standard procedures

ImmunoEM

Early embryos were fixed with 8% PFA in heptane, and after the vitelline membrane was removed by methanol popping, washed and incubated back in PBS with 0.1% BSA. They were then pelletted in 2% agarose in PBS to better visualise the position of embryos in the resin bloc. The structure was very poorly preserved with sucrose embedding and freeze substitution. We obtained better results with progressive low temperature dehydration without sucrose. Embryos were dehydrated in methanol series as follows: 50% at 0°C, 70% at –20°C, 90% at –30°C and 100% at –50°C for 30 minutes each time. Embryos were then embedded in Lowicryl resin (HM20) at –50°C using a Leica AFS device. After polymerisation with UV light at –50°C for 36 hours, ultrathin (80 nm) sections were cut with an ultramicrotome (RMC Mtx), deposited on nickel grids for subsequent staining. The sections were first rehydrated in PBS for 5 minutes at room temperature, blocked with 5% goat serum in PBS for 15 minutes and incubated with the primary antibodies (monoclonal mouse anti HA, 12CA5, Roche, 1/20; or monoclonal mouse anti Lamin/Dm0 1/10, DSHB) overnight at 4°C. After 3 washes (5 minutes each) in PBS, sections were incubated with the secondary antibody (goat anti mouse coupled to colloidal gold particles, 15 nm, Aurion) for 1 hour, washed and the reaction was finally fixed in PBS with 2% glutaraldehyde. Sections were eventually imaged in a Zeiss EM 912 electron microscope and the image acquired with a CCD camera (Gatan Bioscan).

RESULTS

Expression profiling of epithelial morphogenesis

In order to identify new genes involved in epithelial morphogenesis, we selected embryos at successive stages of the process and prepared polyA+ mRNAs to hybridise on microarrays. We sought to obtain homogeneous populations of embryos at each developmental stage in order to increase the temporal resolution of expression profiles. To that end, we hand-selected embryos according to morphological criteria at five time-points (Fig. 1A): before pole cell formation, i.e. before zygotic transcription (T0); during the slow phase (T1) and the fast phase (T2) of cellularisation; and at the beginning (T3) and the end (T4) of gastrulation. Complete microarray data are available in the supplementary material (see Tables S1A-C) and in the GEO databases (http://www.ncbi.nlm.nih.gov/geo/, Series GSE3955). The analysis of the data shows that about 4000 genes are expressed at any of these stages (Table S2). The expression profiles of *nullo*, *Sry*-α, *bnk*, *slam* and *frs* in particular are specifically induced during T1 in agreement with in situ hybridisation data (Fig. 1C,D, Fig. 2; see Tables S1A-C in the supplementary material) (Grosshans et al., 2003; Lecuit et al., 2002; Postner and Wieschaus, 1994; Rose and Wieschaus, 1992; Schejter and Wieschaus, 1993a; Schweisguth et al., 1990; Stein et al., 2002). Other genes are only expressed in T0, T1, T2, T3 or T4 (Table S2). Moreover, the temporal cascade of anteroposterior axis polarity genes is also precisely reconstituted (see Fig. S1 in the supplementary material) (Pankratz, 1993). Three main clusters are revealed: maternal gene, gap gene and segmental polarity gene clusters, whereas primary and secondary pair-rule genes are present

in the last 2 groups. We conclude that these expression data have a very high temporal resolution, revealing rapid (10-15 minute) changes in gene expression with a full range of amplitudes (up to 1000-fold), consistent with a large body of published data.

Precise temporal resolution, highly dynamic changes of expression profiles and high induction allowed us to select genes with increased expression during cellularisation. Nearly 78% (10871) of the *Drosophila* genes (13966) displayed defined expression profiles falling into distinct classes (Fig. 1E). Out of these, 80% (8711) were absent (7232) or downregulated (1479) during the formation of the epithelium, leaving 2160 genes (15% of the total) upregulated during any given stage of epithelial morphogenesis (T1-T4). Clustering allows the identification of distinct sub-classes of gene expression among these 2160 genes (Fig. 1B-D). We could, for example, distinguish genes specifically induced during T1 (slow phase) and/or T2 (fast phase). A surprisingly high number of genes (583, 4%) are shown to be upregulated during cellularisation only (Fig. 1C-E).

We selected from these 2160 genes for functional screening. We applied a number of stringent criteria to yield a reasonable set of genes to be tested. We first focused on genes whose expression during cellularisation (T1 or T2) was at least four times higher than the maternal contribution (T0). Some of them were downregulated later on, but a number showed a sustained expression during

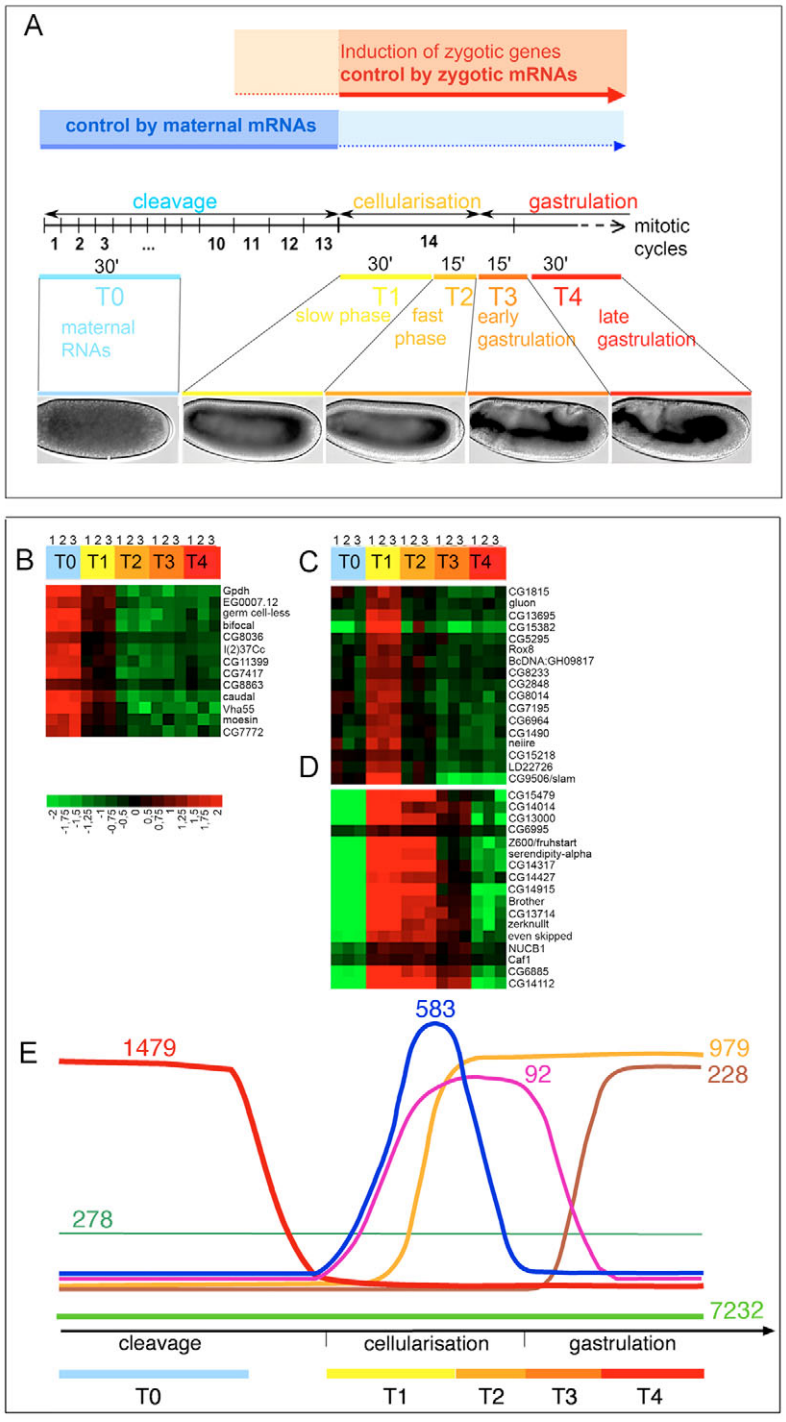

Fig. 1. Different categories of gene expression corresponding to successive stages of early development. (**A**) Early *Drosophila* development showing representative embryos of the five successive stages of epithelium formation and remodelling selected for transcriptome analysis (T0-T4, DIC images, the dorsal side is towards the top and anterior towards the left). (**B-D**) Examples of genes exhibiting a developmental regulation of expression. Increased and decreased expression compared with the mean expression of the five time points (set to 0) for each gene are shown in red and green, respectively. The colour scale ranges from saturated green for log2 ratios –2.0 and below, to saturated red for log2 ratios +2.0 and above. Cluster of genes with a predominant maternal expression (T0, B). Clusters of genes displaying an increased expression in slow phase of cellularisation (T1, C) or throughout cellularisation (T1+T2, D). (**E**) Schematic representation of the different categories of gene expression profiles identified. The variations are only qualitative. The number of genes associated with each category is indicated. Some genes are absent from T0 to T4 (7232, bright green), or display a uniform expression from T0 to T4 (278, dark green).

gastrulation. Indeed we expected that genes involved in polarity or adhesion could have a prolonged requirement and expression during gastrulation. However, we excluded transcription factors, in order to find direct regulators of epithelial formation and polarisation. Finally, we preferentially selected genes with a low maternal contribution, in order to optimise functional studies by RNAi. Using these criteria, we selected 57 novel genes, which are distributed in three main clusters corresponding to different times of peak expression (Fig. 2).

Functional RNAi screen

RNA interference is a very powerful reverse genetics method for the functional dissection of cellular or developmental processes (Boutros et al., 2004; Echard et al., 2004; Eggert et al., 2004; Foley and O'Farrell, 2004; Fraser et al., 2000; Gonczy et al., 2000; Kamath et al., 2003; Kiger et al., 2003; Lum et al., 2003; Sonnichsen et al., 2005). We have used this approach to test the function of the 57 selected genes one by one. Freshly laid embryos were injected with in vitro synthesised dsRNA probes and subsequently screened by time-lapse phase contrast (DIC) microscopy during cellularisation and early gastrulation. An automated system allowed the acquisition of time-lapse data in up to 20 embryos in 2 hours. We could follow with DIC microscopy the coordination of cellularisation with arrest of the cell cycle in interphase 14, nuclear elongation and positioning, lipid droplets transport, membrane invagination and junction integrity through the stability of the newly formed epithelium during gastrulation. Hatching rate (see Table S3 in the supplementary material) and stages of developmental arrest during embryogenesis were also assessed. We recovered striking phenotypes mostly associated with intracellular organisation, falling into five phenotypic classes.

Lipid droplets transport

During cellularisation, lipid droplets undergo two successive phases of polarised transport along microtubules (Welte et al., 1998). First, the net transport of lipid droplets is biased basally towards the plus end of MTs, 'clearing' the apical cytoplasm. Later, during the 'clouding' phase, lipid droplets shift their movement apically towards the minus end of MTs. The movement of lipid droplets along MTs depends on the coordination of motor proteins (Gross et al., 2000; Gross et al., 2002). We identified two genes affecting, respectively, the clearing and the clouding phases. In *CG7428* RNAi embryos, the cytoplasm does not clear and the apical cytoplasm is consequently opaque (see Fig. S2A,A′ in the supplementary material). During the course of our study *CG7428* was shown to encode the gene responsible for the zygotic *halo* phenotype (Gross et al., 2003). Conversely, RNAi to *CG1624*/*dappled* (*dpld*) impaired epithelial clouding, thus mimicking, albeit to a lesser extent, the *klarsicht* (*klar*) phenotype (Fig. S2B,C) (Welte et al., 1998). This phenotype was observed with two distinct dsRNA probes designed against *dpld*. Lipid droplets staining in *dpld* RNAi embryos revealed that the clearing of the cortex was similar to control embryos, whereas the clouding of the newly formed cells was specifically affected (see Fig. S2D in the supplementary material). RT-PCR experiments show that *dpld* is indeed downregulated by RNAi (see Fig. S2E). Moreover, overexpression of *dpld* rescues the clouding phenotype (Fig. S2F).

Nuclear morphogenesis and anchoring

RNAi to *CG5175* leads to an abnormal nuclear behaviour during cellularisation. In control embryos, after the nuclei have elongated along the apicobasal axis, they remain properly aligned until the end of cellularisation. However, in *CG5175* RNAi embryos, the nuclei elongate normally but when the membrane invagination front reaches the basal part of the nuclei, the nuclei lose their proper apical alignment and fall from the cortex following an abnormal apicobasal 'dancing' movement (hence the name *char*) (Fig. 3A-D). At the end of cellularisation, the epithelium adopts a very abnormal organisation, owing to changes in the morphology and position of the nuclei at the cortex. This phenotype is also observed in *char* mutants (see below).

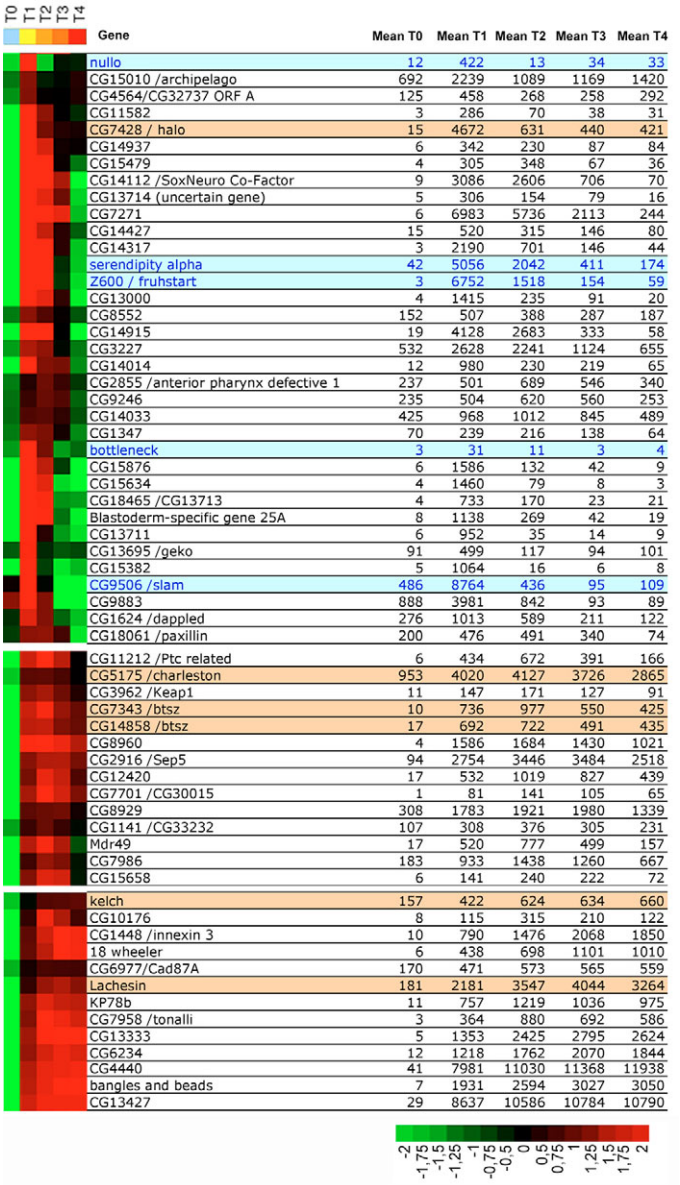

Gene	Mean T0	Mean T1	Mean T2	Mean T3	Mean T4
nullo	12	422	13	34	33
CG15010 /archipelago	692	2239	1089	1169	1420
CG4564/CG32737 ORF A	125	458	268	258	292
CG11582	3	286	70	38	31
CG7428 / halo	15	4672	631	440	421
CG14937	6	342	230	87	84
CG15479	4	305	348	67	36
CG14112 /SoxNeuro Co-Factor	9	3086	2606	706	70
CG13714 (uncertain gene)	5	306	154	79	16
CG7271	6	6983	5736	2113	244
CG14427	15	520	315	146	80
CG14317	3	2190	701	146	44
serendipity alpha	42	5056	2042	411	174
Z600 / fruhstart	3	6752	1518	154	59
CG13000	4	1415	235	91	20
CG8552	152	507	388	287	187
CG14915	19	4128	2683	333	58
CG3227	532	2628	2241	1124	655
CG14014	12	980	230	219	65
CG2855 /anterior pharynx defective 1	237	501	689	546	340
CG9246	235	504	620	560	253
CG14033	425	968	1012	845	489
CG1347	70	239	216	138	64
bottleneck	3	31	11	3	4
CG15876	6	1586	132	42	9
CG15634	4	1460	79	8	3
CG18465 /CG13713	4	733	170	23	21
Blastoderm-specific gene 25A	8	1138	269	42	19
CG13711	6	952	35	14	9
CG13695 /geko	91	499	117	94	101
CG15382	5	1064	16	6	8
CG9506 /slam	486	8764	436	95	109
CG9883	888	3981	842	93	89
CG1624 /dappled	276	1013	589	211	122
CG18061 /paxillin	200	476	491	340	74
CG11212 /Ptc related	6	434	672	391	166
CG5175 /charleston	953	4020	4127	3726	2865
CG3962 /Keap1	11	147	171	127	91
CG7343 /btsz	10	736	977	550	425
CG14858 /btsz	17	692	722	491	435
CG8960	4	1586	1684	1430	1021
CG2916 /Sep5	94	2754	3446	3484	2518
CG12420	17	532	1019	827	439
CG7701 /CG30015	1	81	141	105	65
CG8929	308	1783	1921	1980	1339
CG1141 /CG33232	107	308	376	305	231
Mdr49	17	520	777	499	157
CG7986	183	933	1438	1260	667
CG15658	6	141	240	222	72
kelch	157	422	624	634	660
CG10176	8	115	315	210	122
CG1448 /innexin 3	10	790	1476	2068	1850
18 wheeler	6	438	698	1101	1010
CG6977/Cad87A	170	471	573	565	559
Lachesin	181	2181	3547	4044	3264
KP78b	11	757	1219	1036	975
CG7958 /tonalli	3	364	880	692	586
CG13333	5	1353	2425	2795	2624
CG6234	12	1218	1762	2070	1844
CG4440	41	7981	11030	11368	11938
bangles and beads	7	1931	2594	3027	3050
CG13427	29	8637	10586	10784	10790

Fig. 2. Cluster representation of the 57 selected genes for the RNAi screen together with five genes already known for their role during cellularisation using standard genetic screens (blue). The three different clusters are characterised by a peak induction at early middle and late stages of cellularisation (from top to bottom, respectively). Clustering was made on the mean values of the triplicate experiments for each time-point. The colour scale is the same as in Fig. 1. The genes that showed a distinct phenotype in the RNAi screen are highlighted in orange.

Membrane invagination and cortical organisation

kelch RNAi embryos exhibit, albeit at a low frequency (7%, *n*=88), a broad range of defects at the beginning of cellularisation, including falling of some nuclei from the cortex, a reduction of nuclear elongation and defects in membrane invagination during cellularisation (not shown). Kelch is an actin-binding protein consisting of a BTB/POZ domain and kelch repeats. This phenotype is consistent with the known role of actin in membrane invagination and nuclear anchoring (Foe and Alberts, 1983).

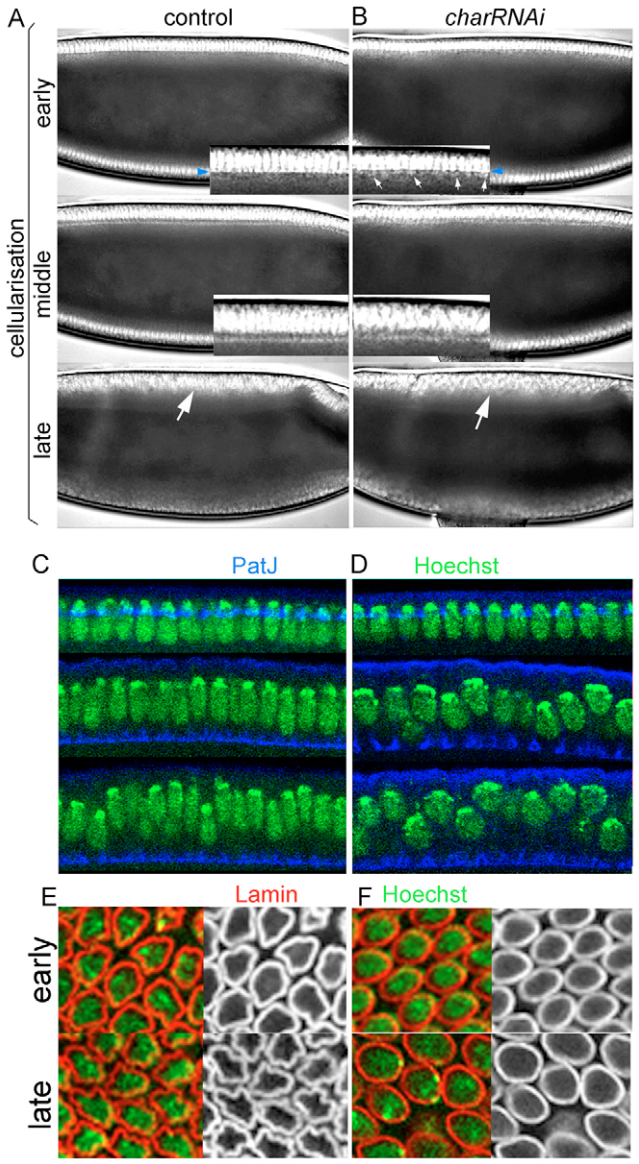

Fig. 3. *CG5175/char* is required for nuclei organisation and apical anchoring. (**A**,**B**) Phase-contrast views of living *Drosophila* embryos at different time intervals. In a control embryo (A), the nuclei (white) elongate and keep a regular organisation until gastrulation (arrow). In a *char* RNAi embryo (B), the nuclei progressively lose their proper apical alignment when the membrane invagination front reaches the basal extent of the nuclei (top, middle and arrows in insets) and acquire an irregular round morphology later (arrow). Blue arrowheads indicate the position of the membrane invagination front in the insets. (**C**,**D**) Confocal images at successive time points of cellularisation in control embryos (C) and *char* RNAi embryos (D). Nuclei are labelled with Hoechst (green) and PatJ (blue) highlights the membrane invagination front. (**E**,**F**) Nuclear envelope (marked with a Lamin antibody, red) and nucleus (green) in control (E) and *char* RNAi embryos (F) at early and late stages of cellularisation and viewed from the top.

Junction stabilisation

We also uncovered defects in the organisation of the epithelium at the end of cellularisation. RNAi against *CG14858/bitesize* (*btsz*), a gene also implicated in growth control (Serano and Rubin, 2003), produces a fully penetrant arrest of gastrulation in that the epithelium no longer elongates along the anteroposterior axis (see Fig. S3 in the supplementary material). This developmental arrest is due to a collapse of the epithelium (not shown). Epithelial cells lose their columnar organisation and become mesenchymal. Different non-overlapping probes produce this phenotype. RT-PCR experiments show that *btsz* is indeed downregulated after RNAi using these different probes. Finally, the phenotype is rescued when *btsz* is overexpressed in RNAi embryos (F.P., J.-M.P., C.L. and T.L., unpublished).

In addition to cellularisation and gastrulation phenotypes, we also noticed late epithelial embryonic defects following RNAi against *Lachesin*. *Lachesin* RNAi led to a fully penetrant lethality associated with profound defects in the development of the tracheal epithelial tubes. Similar epithelial defects were observed in *Lac* mutants (34 homozygote mutant embryos). Characterisation of *Lachesin* involvement in tracheal development has been reported since then (Llimargas et al., 2004).

We shall focus in the following part on *char*, a new regulator of nuclear morphogenesis important for epithelial organisation in the embryonic epithelium.

char, a new regulator of nuclear morphogenesis and anchoring

In *char* RNAi embryos, the nuclei fall from the cortex midway through cellularisation, as the invaginating membrane reaches the basal extent of the nuclei (Fig. 3A-D). The earliest defect in nuclear positioning appears as an irregularity in the alignment of the nuclei. Precise measurements show that nuclear growth and elongation are normal during slow phase. At the beginning of cellularisation, the nuclei are spherical (5 μm in diameter). They subsequently elongate along the apicobasal axis and become ellipsoid with a long axis of 9 μm and a small axis of 5 μm. The same measurements are obtained in *char* RNAi embryos. However, during fast phase, the morphology of control and *char* RNAi nuclei becomes very different. In controls, the nuclei reduce a bit their small axis to 4 μm and slightly elongate to 10 μm (Fig. 3C). Deep infoldings of the nuclear envelope (NE) accompanies this further change in nuclear shape (Fig. 3E). However, *char* RNAi nuclei become spherical instead of elongated (Fig. 3D), without infolding of the NE (Fig. 3F). Their diameter is on average 6.8 μm instead of 5 at the onset of cellularisation, reflecting the expansion of the NE during slow phase (about twofold increase in surface area from ~300 μm^2 to ~600 μm^2), as in control embryos.

A similar, albeit slightly weaker, nuclear phenotype is observed in *char* mutant embryos ($char^{EY0769}$: 40%, *n*=45 of the embryos from homozygous parents). $char^{EY0769}$ is a hypomorphic *char* allele resulting from a P-element insertion in the intron of one of the two *char* isoforms (that only differ in the 5′UTR sequence, see Fig. S4 in the supplementary material). RT-PCR experiments reveal that one of the two *char* isoforms is removed in $char^{EY0769}$ mutant embryos (Fig. S4), resulting in lower expression of *char* transcripts. In embryos homozygous for a deficiency that completely removes the zygotic contribution of *char*, we also see a clear phenotype (Fig. 7D,F; *Dfchar*: 30%, *n*=55 of the embryos from heterozygous

parents). A similar phenotype is also observed in *Dfchar/char*^{EY0769} embryos (see Fig. S5 in the supplementary material, embryos from homozygous *char*^{EY0769} females crossed to heterozygous *Dfchar*/+ males, 40%, *n*=40).

Several lines of evidence show that *char* is, as expected from its induction during cellularisation, required zygotically, although we can also detect a maternal effect. Twenty percent (*n*=85) of embryos laid by *Dfchar/char*^{EY0769} females crossed to *OreR* control males display a nuclear phenotype. In addition, 55% of the embryos now display the mutant phenotype when the same females are crossed to homozygous *char*^{EY0769} males (*n*=74). Finally, all embryos are wild type when *OreR* females are crossed to homozygous *char*^{EY0769} males (0% mutant phenotype, *n*=68).

The expression of Char is strongly reduced in *Dfchar* mutant embryos (see Fig. 7A-F), the remaining low levels of Char in deficiency embryos derives from the maternally produced Char. Char is not detected in *char* RNAi embryos, suggesting that RNAi to *char* inhibits both the maternal and zygotic contributions, explaining the stronger nuclear phenotype observed in such embryos.

Impact of nuclear defects on epithelial organisation

The rounding up of nuclei in *char*-depleted embryos is accompanied by a distortion of cell shape in the epithelium at the end of cellularisation and in the gastrula (Fig. 4). We labelled embryos with phalloidin (red) and PatJ (green) to mark the cell surface and apical junctions together with nuclei (blue). In control embryos, the primary embryonic epithelium is columnar as the cells have a regular section along the apicobasal axis (Fig. 4A,B, compare sections z1 and z2). Moreover, all the cells have a similar surface area in cross-section (Fig. 4B). In *char*-depleted embryos, however, the epithelium is no longer columnar and becomes pseudo-stratified. Epithelial cells adopt a bottle shape along the apicobasal axis (Fig. 4C) and the section area of the cells is very irregular (Fig. 4D), often reduced by half compared with wild-type cells in regions devoid of nuclei (compare Fig. 4B,D, arrows) or expanded in the presence of large round nuclei (Fig. 4D, arrowheads). The irregular packing of cells in response to nuclear bulging sometimes disrupts the regular organisation of the apical surface and junctions of cells (Fig. 4D, z2).

Together, these data suggest that Char constrains nuclear shape along the apicobasal axis in order to maintain the regular columnar morphology of cells during gastrulation.

Nuclear envelope association with microtubules and centrosomes in *char* RNAi embryos

Cytoskeletal elements, in particular microtubules, control the localisation and morphology of the nuclei. Actin or microtubule depolymerisation produces defects in apical nuclear anchoring during cellularisation (Fig. 5A) (Foe et al., 1993; Schejter and Wieschaus, 1993b). Moreover, the nuclei also round up when microtubules are depolymerised (not shown). Defects observed in *char*-depleted embryos thus suggested that Char might regulate actin or microtubules. However, phalloidin staining did not reveal any defect in cortical actin organisation in *char* RNAi embryos (not shown). Moreover, serial confocal sections of embryos stained with an antibody to α-tubulin also revealed no apparent defect in the apicobasal organisation of MTs. In the wild type, astral MTs extend from the centrosomes towards the apical surface (Fig. 5B,D,I) and form a dense apical network (Fig. 5B). Another population of MTs extends basally surrounding the nuclei and in tight association with the NE (Fig. 5B). This population of MTs is believed to constrain

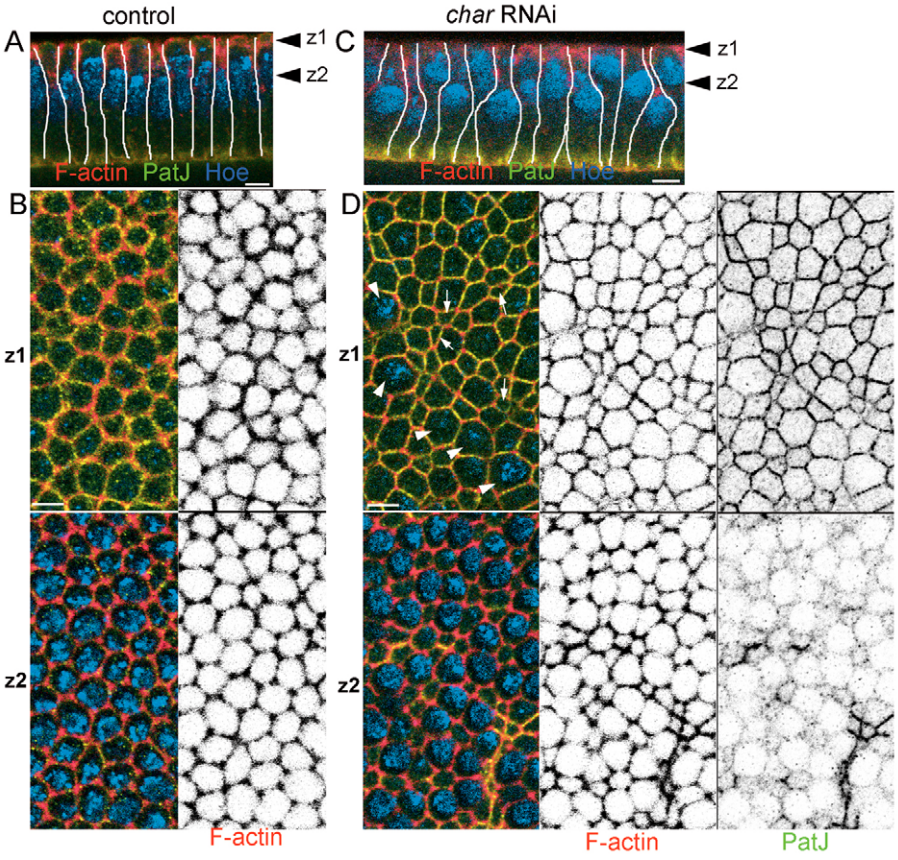

Fig. 4. Defects in epithelial organisation associated with unconstrained nuclear shape in *char* RNAi embryos. Sections showing phalloidin, a marker of F-actin (red), the apical protein Patj (green) and the nuclear dye Hoechst (blue) in control (**A**,**B**) and *char* RNAi (**C**,**D**) embryos at the end of cellularisation, viewed from the side (A,C) and from the top (B,D). The white lines define the cell contour determined by the localisation of phalloidin and PatJ. In B and D, z1 and z2 are, respectively, apical and more lateral sections indicated in A and C. The apicobasal morphology of cells is regular in control embryos. In *char* RNAi embryos, cell shape is irregular: many cells display a small apical section (D, arrows) and others have a larger apical section when the nuclei are located apically (D, arrowheads). Apical markers (PatJ) are abnormally present in the deeper section z2 (D), indicating defects in junctional organisation in *char* RNAi embryos. Scale bar: 5 μm.

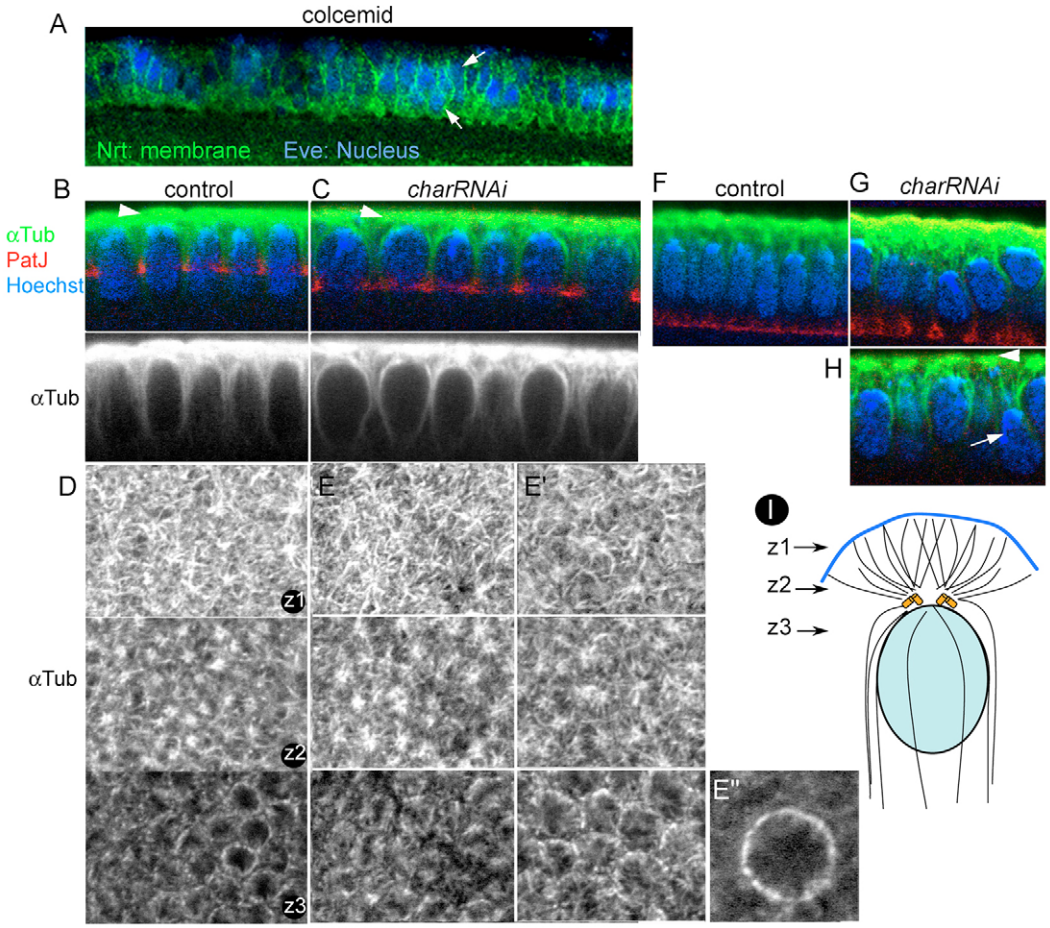

Fig. 5. Microtubules organisation in control and *char* RNAi embryos. (**A**) Nuclear localisation during cellularisation after injection of colcemid to depolymerise microtubules (MTs). Neurotactin (green) marks the plasma membrane, Even-skipped (blue) labels the nuclei. Arrows indicate misaligned nuclei. (**B-H**) MTs organisation in control (B,D,F) and *char* RNAi (C,E,E′,G,H) embryos, during early (B,C) and late (F-H) cellularisation. MTs (α-tubulin) are in green, nuclei (Hoechst) are in blue and the membrane invagination front (Patj) is in red. Arrowheads show apical astral microtubules. The white arrow indicates a falling nucleus in *char* RNAi embryo in H. (D-E′) Grazing sections showing astral MTs in the control (D) and *char* RNAi (E,E′) embryos. Section planes (z1-z3) are schematised in **I**. (E′′) Detail of a grazing section at z3 of the bottom nucleus shown in H.

nuclear shape. Grazing sections show that both apical astral MTs (Fig. 5D,E,E′) and the tight association between MTs and the NE (section z3 in Fig. 5E and E′, and Fig. 5E′′) are, however, normal in *char* RNAi embryos.

Nuclei that have already fallen from the cortex do not fall together with apical astral MTs which remain anchored at the cortex (Fig. 5G,H). Together, these data argue that *char* controls neither cortical actin nor MTs per se, or the interaction between cortical actin and astral MTs, but the interaction between the NE and the microtubule organising centre, i.e. the centrosomes.

Strikingly, even before nuclei can be seen to fall from the cortex, in *char* RNAi embryos the centrosomes (labelled with γ-tubulin), are not properly aligned apically and do not show a tight association with the NE, unlike in control embryos (Fig. 6A,B). This defect becomes stronger as the nuclei fall out (Fig. 6B′ and B′′) and at the end of cellularisation, the dissociation between centrosomes and nuclei is very pronounced. We noticed that most of the times only one centrosome is dissociated from the NE, reflecting a possible difference between the two centrosomes at this stage. The fact that the centrosome defect is observed before the nuclei fall out, argues that Char may primarily control the organisation of the NE, thereby affecting its interaction with centrosomes. Our data thus argue that the nuclear fall-out phenotype stems from a disruption of this interaction, and not the opposite.

We conclude that Char controls nuclear morphology of the NE, as well as its surface properties, which are required for its interaction with centrosomes. To gain further insight into the mechanism of Char function, we looked at its subcellular localisation.

Char is farnesylated and membrane anchored at the NE

Char is a 570 amino acid protein with a Coiled-coil domain (amino acids 143-190) and a farnesylation site (CSIM motif) at the C terminus. Farnesylation is commonly used to anchor a protein in a phospholipid bilayer, such as the NE (Zhang and Casey, 1996). For example, Lamin (also known as Dm0), which accumulates at the inner nuclear membrane, is farnesylated (Mounkes et al., 2003). Antibodies raised against a C-terminal peptide of Char reveal a striking localisation of Char at the NE in early embryos and all other developmental stages inspected (Fig. 7A; data not shown). This distinct localisation is lost in *char* RNAi embryos and is greatly reduced in embryos bearing a deficiency for *char* (*Dfchar*), in which maternally expressed Char is present (Fig. 7A-F).

Char localisation at the NE supports our conclusion that Char controls early nuclear morphology and the interaction between the NE and centrosomes. We tested the possibility that Char is farnesylated and that this may be essential for its localisation at the NE and, as a result, for its function. We first checked that Char is anchored via its farnesylation group by comparing the localisation of HA-tagged full length Char (at the N terminus, HA-Char) and a form of Char devoid of the CSIM farnesylation motif (HA-CharΔCSIM). These proteins were expressed in early embryos. HA-Char localises at the NE like the endogenous protein (Fig. 8A). By contrast, HA-CharΔCSIM is almost completely removed from the NE and correspondingly accumulates in the cytoplasm and the nucleoplasm (Fig. 8B). This suggests that the farnesylation motif is required for proper nuclear localisation of Char. In order to show

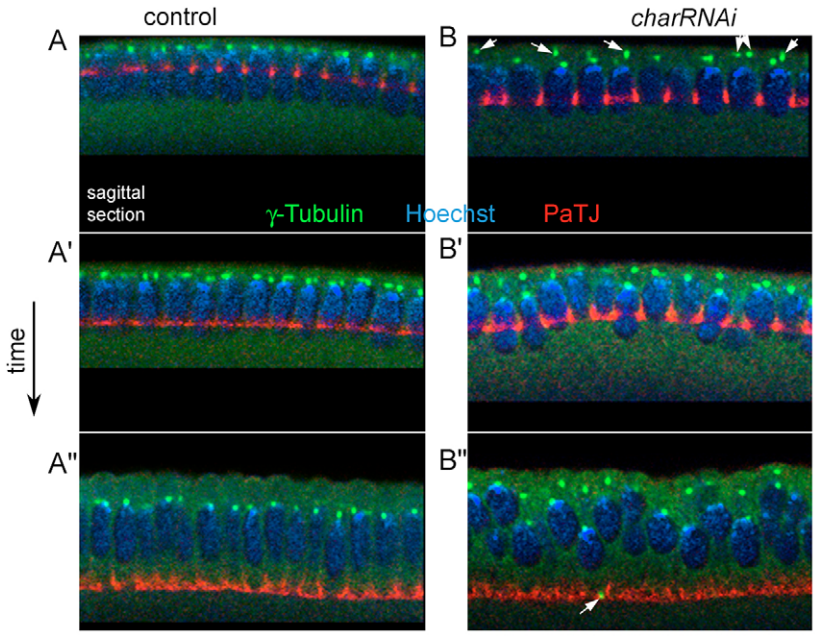

Fig. 6. *char* controls centrosomes association with nuclei. Sagittal sections of control (**A-A**′′) and *char* RNAi embryos (**B-B**′′) at successive time points of cellularisation showing centrosomes (γ-tubulin) in green, membrane invagination front (Patj) in red and nuclei (Hoechst) in blue. Arrows indicate centrosomes detached from the nuclei in *char* RNAi embryos.

more directly that Char is farnesylated, we treated S2 cells expressing HA-Char with increasing concentrations of the farnesyltransferase inhibitor FTI-277 (10-40 μM). In contrast to cells not exposed to FTI-277, after 24 hours exposure to this inhibitor, HA-Char appears on western blot as a doublet (Fig. 8C, left). As the concentration of FTI-277 increases, the faster migrating fraction (Fig. 8C, lower band, arrow) increases with respect to the slower fraction (upper band). The fast migrating fraction represents non-farnesylated HA-Char as HA-CharΔCSIM migrates at the same position irrespective of the presence of FTI-277 (Fig. 8C, right). We conclude that Char is farnesylated.

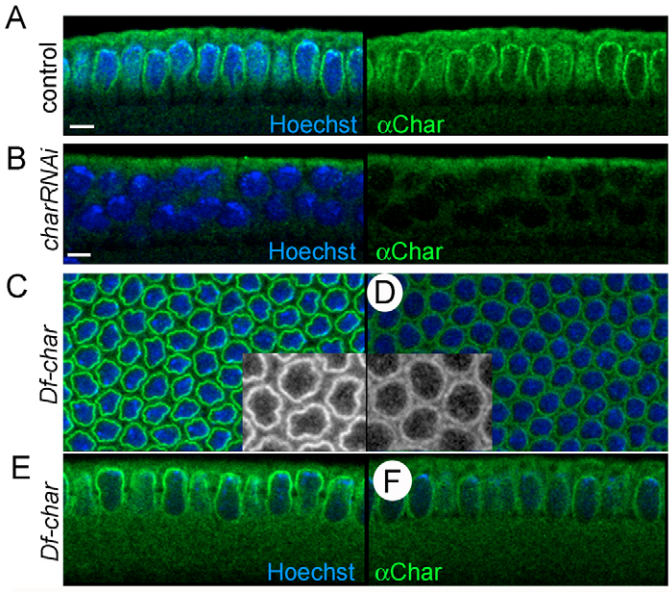

Fig. 7. Char localises to the nuclear envelope. (**A**,**B**) Char antibody staining (green) highlights the nuclear envelope during cellularisation in a control embryo (A) but is absent in a *char* RNAi embryo (B). (**C-F**) Char staining in embryos from heterozygous flies for a deficiency covering the *char* locus (*Dfchar*), viewed from the top (C,D, insets) and in sagittal sections (E,F). Two categories of embryos, inferred to be, respectively, homozygous *DfChar* embryos and heterozygous siblings, are observed: in the first, the nuclei have a normal morphology and high levels of Char at the NE (C,E); in the second, the nuclei display the distinct *char*RNAi nuclear envelope phenotype together with a low expression of Char (D,F). Scale bars: 5 μm.

To confirm the farnesylation of Char in vivo and test the function of this modification, we then injected FTI-277 in early embryos (10-20 μM final concentration). Time lapse recording of embryos during cellularisation showed a striking and penetrant (95%, *n*=54) phenotype undistinguishable from *char* RNAi (Fig. 8D): the nuclei round up and fall from the cortex at the same time as in *char* RNAi. This is also apparent in confocal sections showing the aberrant nuclear morphology (Fig. 8E). In these conditions, Char is no longer present at the NE (Fig. 8F, right). Interestingly, however, Lamin localisation is not affected during cellularisation (Fig. 8F, right), probably owing to the stability of its maternal contribution.

We conclude that Char is farnesylated. This farnesylation is required for its localisation at the NE and is essential for its function in nuclear morphogenesis and anchoring.

Char is localised at the inner nuclear membrane together with Lamin

The nuclear envelope is composed of an inner and an outer membrane. Farnesylation can potentially anchor protein to either membrane. For example, Lamin/Dm0, is farnesylated and localises to the inner membrane. High-resolution confocal imaging reveals that Char co-localises with Lamin at the NE (Fig. 9A,B), suggesting that Char may in part localise to the inner membrane. To further test this, we compared the localisation of Char and wheat germ agglutinin (WGA), a marker of the nuclear pores. Char (red) and WGA (green) co-localise (Fig. 9C-D′, arrowheads) but Char is also clearly detected alone in a more internal region of the NE (Fig. 9C-D′, arrows). These data argue that Char localises in the inner nuclear membrane of the NE, and possibly also in the outer membrane. We confirmed this using immunoelectron microscopy (IEM) to localise HA-Char and Lamin. The NE was identified at the boundary between the cytoplasm and the nucleoplasm that have different

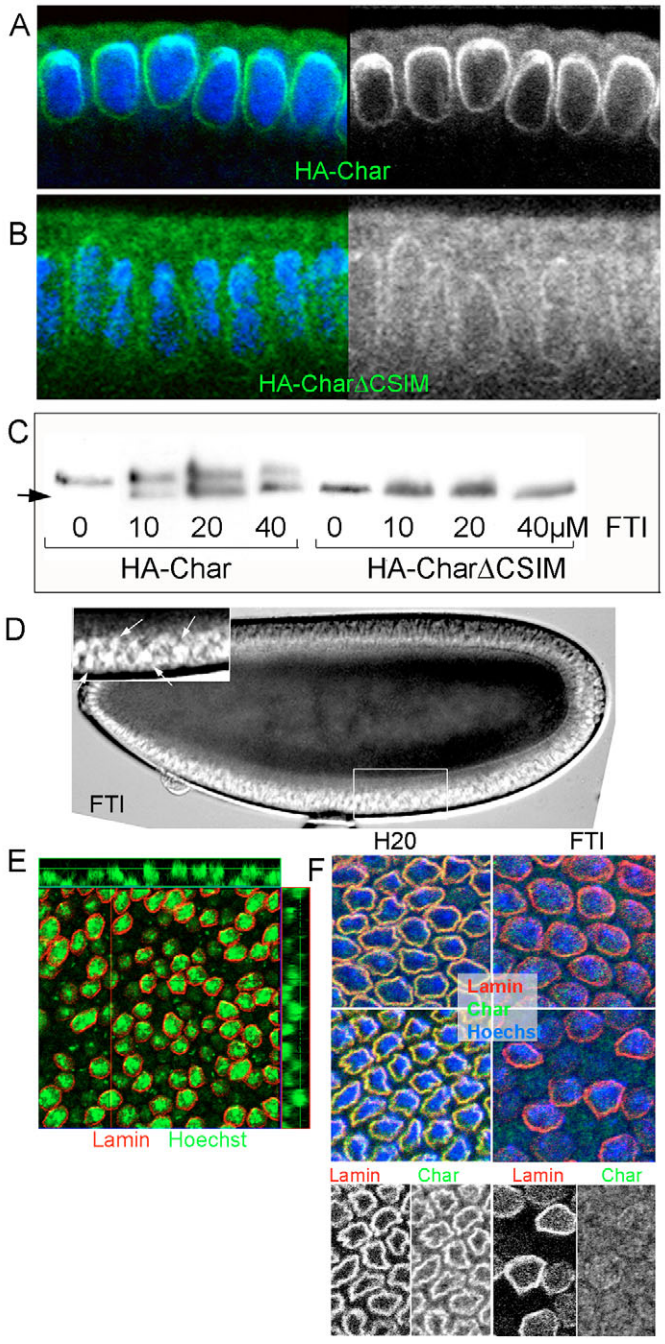

Fig. 8. Char is farnesylated. (**A**,**B**) HA-Char localises to the nuclear envelope in a cellularising embryo (A), whereas a Char mutant protein deleted of the farnesylation motif CSIM (HA-CharΔCSIM) is mostly present in the cytoplasm and the nucleoplasm, although traces are detected at the NE (B). (**C**) Western blot showing the different migration on SDS-PAGE of HA-Char and HA-CharΔCSIM from the lysate of *Drosophila* S2 cells in the absence or presence of 10 to 40 μM of the farnesyl-transferase inhibitor FTI-277. The arrow indicates the position of the fast migrating, non-farnesylated fraction of Char (lower band). (**D**) Injection of FTI-277 60 minutes prior to cellularisation causes a '*char*-like' phenotype: the nuclei round up and fall from the cortex. The inset shows a detailed view of the boxed area. The nuclei (in white) are not properly anchored apically (arrows). (**E**) Confocal section from the top showing the nuclear morphology and position with Hoechst (green) and Lamin (red). *z*-stack projections are shown at the top and to the right showing the abnormal positions of the nuclei viewed from the side. (**F**) In FTI-injected embryos during cellularisation (right), Char is no longer present at the NE compared with control water-injected embryos (left), whereas Lamin localisation is not affected yet.

electron densities (Fig. 9E). Quantification of immunogold particles to localise HA-tagged Char and Lamin revealed a striking enrichment of both HA-Char (70%, *n*=127) and Lamin (65%, *n*=26) at the NE, although a fraction is also present in the nucleoplasm (20 and 30% respectively) (Fig. 9E,H). We determined the position of the Lamin and HA-Char gold particles with respect to the NE at the boundary between the nucleoplasm and cytoplasm, and find a clear bias towards the nucleoplasmic side of the NE for both proteins (Fig. 9F-H). We point out that Lamin and Char have very similar distributions.

Although this shows that Char is at the inner membrane, we could not exclude the possibility that traces of Char may be also found at the outer membrane. We thus performed a final experiment in which we compared the localisation of Char and Lamin in S2 cells in which we permeabilised only the plasma membrane (40 μg/ml digitonin) or all membranes (0.1% Triton X100). Although in the latter case both Lamin and Char were detected at the NE (Fig. 9I), in the presence of digitonin, no labelling was observed at the NE although the cytoplasmic staining of Char was detected, indicating that antibody penetration through the plasma membrane was normal in these conditions (Fig. 9J).

Together we conclude that Char is localised strictly at the inner nuclear membrane. Char and Lamin share similar localisations and targeting mechanisms. The localisation of Char at the inner nuclear membrane suggests that Char participates in the organisation of a robust nucleoskeleton that is able to structure the nuclear envelope in tightly packed epithelial cells in response to microtubules.

DISCUSSION

Our analysis of gene regulation during cellularisation and subsequent functional tests identify new regulators of cellular architecture in the developing *Drosophila* epithelium. The approach proves successful in identifying cellular pathways underlying the developmental control of tissue morphogenesis in the embryo. We identify one such pathway controlling nuclear morphogenesis through the upregulation of *char*. Our data show the importance of nuclear morphogenesis on epithelial organisation during development.

Efficiency of the functional screen

Although standard genetic screens have proven very powerful to identify many genes required for *Drosophila* embryonic development using static pictures of development such as the morphology of the cuticle, it has long been appreciated that such blind approaches could not be used to screen systematically dynamic developmental processes using time-lapse recordings. However, aneuploid screens have proven a very good alternative to find purely zygotic loci whose deletion produces strong phenotypes during early development (Merrill et al., 1988; Wieschaus and Sweeton, 1988). Many loci originally identified have been cloned (Lecuit et al., 2002; Postner and Wieschaus, 1994; Rose and Wieschaus, 1992; Schejter and Wieschaus, 1993a; Schweisguth et al., 1990; Stein et al., 2002). In some cases, however, cloning approaches have been difficult, and some loci remain uncloned.

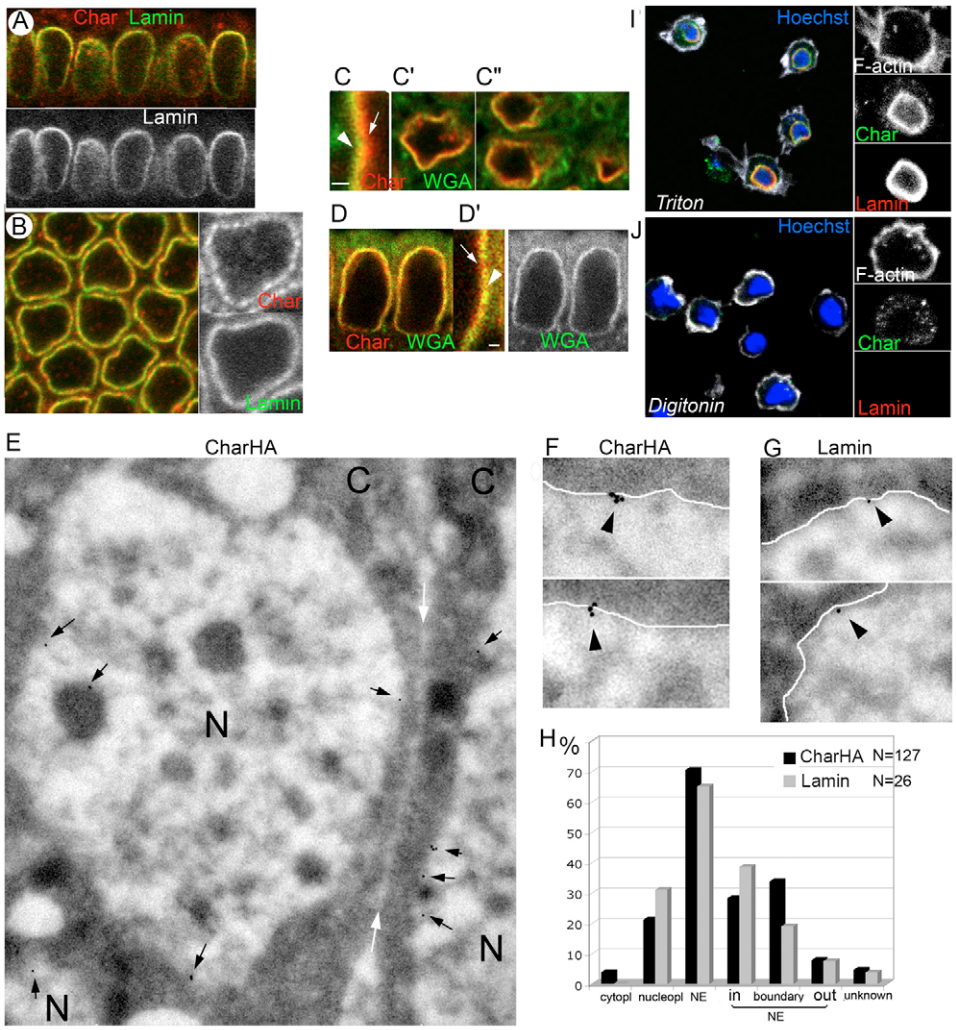

Fig. 9. Char is localised at the inner nuclear membrane. (**A**,**B**) Localisation of Char (red) and Lamin (green) in the NE of embryos viewed in sagittal sections (A) and from the top (B). (**C**,**D**) WGA (green) and Char (red) localisation at the NE of embryos viewed from the top (C-C′′) and in sagittal sections (D,D′). C shows a detail of C′ and D′ a detail of D. Scale bars: 5 μm, except in C,D′ (300 nm). (**E**-**H**) Immunogold localisation of HA-Char (black arrows) in an early embryo. The nucleoplasm (N) and cytoplasm (C) of three different cells are indicated and have very different electron density. The white arrows indicate contacting cell surfaces. HA-Char is concentrated at the NE. High magnification views of representative localisation at the NE are shown in F, where the white line defines the position of the NE. (G) Representative localisation of Lamin. (H) Quantification of the localisation of HA-Char and Lamin. We positioned the NE at the boundary between the nucleoplasm and cytoplasm (white lines in F and G show examples) and determined the localisation of gold particles (15 nm) at the boundary, or the inner (in) or outer (out) side of the NE. Lamin and HA-Char are distributed similarly, and are particularly biased towards the inner side of the NE. (**I**,**J**) S2 cells stained with Char (green), Lamin (red), Hoechst (blue) and Phalloidin (white) to mark F-actin at the cell cortex after permeabilisation with Triton (I) or digitonin (J). Char staining is absent from the NE when the plasma membrane but not the NE is permeabilised (with digitonin).

To try to overcome these difficulties, we developed an alternative approach combining accurate gene expression profiling of early development and a functional screen using RNAi. We here present exhaustive and accurate expression profiles of the whole genome with a high temporal resolution allowing us to select a limited number of genes with a higher chance of being functionally required than would offer a blind screen. This selection allowed us to conduct a very accurate time-lapse assessment of phenotypes, with the possibility of scoring directly a broad range of defects during cellularisation and gastrulation. A large time-lapse data set was collected to carefully analyse and quantify even subtle phenotypes (e.g. a mild reduction in membrane invagination). In practice, over 10% (6/57) of the genes tested indeed showed a striking phenotype. Apart from *kelch,* we focussed only on very penetrant phenotypes (>80%).

Developmental control of nuclear organisation

One of the major outcomes of this screen is the identification, with *char,* of a developmental control of nuclear shape in embryos. *char* was identified based on its upregulation during cellularisation, although its expression is maintained later during development and the gene is also contributed to maternally. Before cellularisation, the dividing nuclei are round spheres. As cellularisation proceeds, the nuclei first elongate and later maintain the apicobasal elongation and infolded structure in epithelial cells. In *char*-depleted embryos, the nuclei elongate but fail to maintain this constrained shape and become rounded instead (Fig. 3). The bulging of nuclei disrupts the regular columnar organisation of cells and distorts cell shape (Fig. 4). Thus, the developmental induction of *char* controls nuclear shape in the context of epithelial morphogenesis. This clearly shows that,

contrary to a naïve expectation, cell morphology does not constrain nuclear shape, but rather that nuclear morphogenesis is controlled by a local and specific mechanism so that cell shape is preserved. Char provides an entry point in this process.

Although MTs control nuclear morphogenesis, we also showed that, to our surprise, the function of Char is independent of MTs interaction with the NE. When Char is depleted, MTs still bind properly to the NE (Fig. 5). This suggests that, although necessary, MTs are not sufficient to constrain nuclear morphogenesis and that Char is required to let MTs shape the NE properly.

What are the mechanisms of Char function? The earliest defects observed when *char* is downregulated are an absence of infolding of the NE together with a dissociation of the NE with the centrosomes. Later, the nuclei lose their elongated and constrained morphology, round up, fall from the cortex and consequently distort cell shape. The sequence of events, as the phenotype unfolds, thus points to a direct role of Char at the NE. In agreement with this, we show that Char localises at the inner nuclear membrane of the NE and that farnesylation of Char provides a lipid anchor required for its localisation and for its function. This suggests two possible mechanisms. Char may directly control the structural organisation of the NE and thereby indirectly affect attachment to centrosomes. Alternatively, Char may primarily regulate centrosome-NE interaction. The fact that Char affects NE morphogenesis and is localised at the inner nuclear membrane together with Lamin, supports the former possibility and argues that Char is a component of a nucleoskeleton required to respond to MTs in the inner nuclear membrane. Supporting the idea that Char may form a structural scaffold at the inner NE, immunofluorescence labelling with a Char antibody reveals small protein clusters (Fig. 9B, top inset) that are also evident and more striking in immunogold labelling (Fig. 9F). Interestingly, we found that HA-Char can be pulled down on GST-Char beads (using GST-pull down assays, see Fig. S6 in the supplementary material) arguing that multiple Char proteins can form a complex. This could contribute to the scaffolding properties of Char as for Lamins, which are known top dimerize.

The *char* phenotype is also reminiscent of the *unc-83/unc-84* and *zyg-12* phenotypes of *C. elegans* embryos. UNC-83 and UNC-84 localise to the NE and ensure the correct positioning of the nuclei, probably via interactions with MTs (Gruenbaum et al., 2005; Starr et al., 2001). ZYG-12 localises to the centrosomes and the NE and controls the attachment of the centrosomes to the male pronucleus. ZYG-12 interacts with a dynein chain (DLI-1) (Malone et al., 2003). No functional orthologues of *unc-83/-84* and *zyg-12* have been described in *Drosophila*. However, Lis1 and Klarsicht, both of which regulate Dynein, have been implicated in nuclear positioning, in particular during eye imaginal disc morphogenesis but not in early embryos (Guo et al., 2005; Mosley-Bishop et al., 1999; Swan et al., 1999; Welte et al., 1998). Interestingly, the inactivation of Dynein during cellularisation after injection of blocking antibodies causes a phenotype partly reminiscent of *char* loss of function, in that the nuclei round up and lose their apical alignment (Papoulas et al., 2005) (John Sisson, personal communication). Moreover, centrosome-NE attachment is also compromised in dynein mutant embryos (Robinson et al., 1999). We propose that the role of Char in NE organisation provides a link with such a machinery. Although *char* does not appear to regulate microtubules interaction with the NE, the membrane association of Char may indeed control the assembly of a structural scaffold that indirectly couples to microtubules across the NE. Analogous to the morphogenesis of the plasma membrane, where membrane associated proteins form large scaffolds that couple the internal actin filaments to external matrix proteins, Char may link the structural protein Lamin inside the nucleus to 'external', cytoplasmic microtubules. This mechanism may also explain how the polarised organisation of microtubules directs the polarised constrained morphology of nuclei controlled by Char. Determining the structural link between the outer nuclear membrane to which MTs bind and the inner nuclear membrane where Char and Lamin structure the NE will require the identification of Char molecular partners and of other genes with similar phenotypes. Interestingly, after injection of α-amanitin (an inhibitor of pol-II transcription and hence of zygotic induction) prior to cellularisation, the nuclei display a typical *char*-like phenotype but the association of MTs with the NE is lost (T.L., unpublished), indicating that other zygotic genes control the link between MT and NE morphogenesis. Cellularisation thus provides a particularly interesting system with which to study the developmental control of nuclear morphogenesis.

A broad family of diseases called laminopathies are caused by defects in the organisation of the NE in vertebrates (Gruenbaum et al., 2005; Mounkes et al., 2003). Identifying molecular partners of Char and genes required for NE morphogenesis may thus shed light on the developmental pathway underlying NE in *Drosophila* and on these poorly understood diseases.

We are especially grateful to Marc Hild and Renato Paro, who generously provided us with the PCR clones of the selected genes; and to Christelle Thibault (IGBMC, Génopôle, Strasbourg), who coordinated the Affymetrix microarrays experiments. We also thank Thien-Phong Vu Manh and Samuel Granjeaud for bioinformatics assistance; Véronique Morel for suggesting the *char* name; Michael Welte for flies; Hugo Bellen, Manzour Bhat, Dan Kiehart, David Kosman and John Reinitz for antibodies; and Sébastien Darras for sharing Bodipy. We also thank Steve Kerridge for comments on the manuscript. This work was supported by the Association pour la Recherche contre le Cancer (ARC, subvention libre 5179), the Ministère de la Recherche (Réseau National des Génopôles, Programme Affymetrix), the CNRS (ATIPE grant), the Fondation pour la Recherche Médicale (FRM), the EMBO Young Investigator Programme and the Fondation Schlumberger pour l'Education et la Recherche (FSER). F.P. was supported by the CNRS (bourse BDI) and by the Académie de médecine. C.L. was supported by the FSER.

Supplementary material

Supplementary material for this article is available at
http://dev.biologists.org/cgi/content/full/133/4/711/DC1

References

Arbeitman, M. N., Furlong, E. E., Imam, F., Johnson, E., Null, B. H., Baker, B. S., Krasnow, M. A., Scott, M. P., Davis, R. W. and White, K. P. (2002). Gene expression during the life cycle of Drosophila melanogaster. *Science* **297**, 2270-2275.

Boutros, M., Kiger, A. A., Armknecht, S., Kerr, K., Hild, M., Koch, B., Haas, S. A., Consortium, H. F., Paro, R. and Perrimon, N. (2004). Genome-wide RNAi analysis of growth and viability in Drosophila cells. *Science* **303**, 832-835.

Cox, R. T., Kirkpatrick, C. and Peifer, M. (1996). Armadillo is required for adherens junction assembly, cell polarity, and morphogenesis during Drosophila embryogenesis. *J. Cell Biol.* **134**, 133-148.

Desbordes, S. C. and Sanson, B. (2003). The glypican Dally-like is required for Hedgehog signalling in the embryonic epidermis of Drosophila. *Development* **130**, 6245-6255.

Echard, A., Hickson, G. R., Foley, E. and O'Farrell, P. H. (2004). Terminal cytokinesis events uncovered after an RNAi screen. *Curr. Biol.* **14**, 1685-1693.

Eggert, U. S., Kiger, A. A., Richter, C., Perlman, Z. E., Perrimon, N., Mitchison, T. J. and Field, C. M. (2004). Parallel chemical genetic and genome-wide RNAi screens identify cytokinesis inhibitors and targets. *PLoS Biol.* **2**, E379.

Foe, V., Odell, G. and Edgar, B. (1993). Mitosis and morphogenesis in the *Drosophila* embryo: point and counterpoint. In *The Development of Drosophila melanogaster*, vol. 1 (ed. A. Martinez Arias and M. Bate), pp. 149-300. New York: Cold Spring Harbor Laboratory Press.

Foe, V. E. and Alberts, B. M. (1983). Studies of nuclear and cytoplasmic behaviour during the five mitotic cycles that precede gastrulation in Drosophila embryogenesis. *J. Cell Sci.* **61**, 31-70.

Foley, E. and O'Farrell, P. H. (2004). Functional dissection of an innate immune response by a genome-wide RNAi screen. *PLoS Biol.* **2**, E203.

Fraser, A. G., Kamath, R. S., Zipperlen, P., Martinez-Campos, M., Sohrmann,

M. and Ahringer, J. (2000). Functional genomic analysis of C. elegans chromosome I by systematic RNA interference. *Nature* **408**, 325-330.
Gonczy, P., Echeverri, C., Oegema, K., Coulson, A., Jones, S. J., Copley, R. R., Duperon, J., Oegema, J., Brehm, M., Cassin, E. et al. (2000). Functional genomic analysis of cell division in C. elegans using RNAi of genes on chromosome III. *Nature* **408**, 331-336.
Gross, S. P., Welte, M. A., Block, S. M. and Wieschaus, E. F. (2000). Dynein-mediated cargo transport in vivo. A switch controls travel distance. *J. Cell Biol.* **148**, 945-956.
Gross, S. P., Welte, M. A., Block, S. M. and Wieschaus, E. F. (2002). Coordination of opposite-polarity microtubule motors. *J. Cell Biol.* **156**, 715-724.
Gross, S. P., Guo, Y., Martinez, J. E. and Welte, M. A. (2003). A determinant for directionality of organelle transport in Drosophila embryos. *Curr. Biol.* **13**, 1660-1668.
Grosshans, J., Muller, H. A. and Wieschaus, E. (2003). Control of cleavage cycles in Drosophila embryos by fruhstart. *Dev. Cell* **5**, 285-294.
Gruenbaum, Y., Margalit, A., Goldman, R. D., Shumaker, D. K. and Wilson, K. L. (2005). The nuclear lamina comes of age. *Nat. Rev. Mol. Cell. Biol.* **6**, 21-31.
Guo, Y., Jangi, S. and Welte, M. A. (2005). Organelle-specific control of intracellular transport: distinctly targeted isoforms of the regulator Klar. *Mol. Biol. Cell* **16**, 1406-1416.
Kamath, R. S., Fraser, A. G., Dong, Y., Poulin, G., Durbin, R., Gotta, M., Kanapin, A., Le Bot, N., Moreno, S., Sohrmann, M. et al. (2003). Systematic functional analysis of the Caenorhabditis elegans genome using RNAi. *Nature* **421**, 231-237.
Kiger, A. A., Baum, B., Jones, S., Jones, M. R., Coulson, A., Echeverri, C. and Perrimon, N. (2003). A functional genomic analysis of cell morphology using RNA interference. *J. Biol.* **2**, 27.
Lecuit, T. (2004). Junctions and vesicular trafficking during Drosophila cellularization. *J. Cell Sci.* **117**, 3427-3433.
Lecuit, T. and Wieschaus, E. (2000). Polarized insertion of new membrane from a cytoplasmic reservoir during cleavage of the Drosophila embryo. *J. Cell Biol.* **150**, 849-860.
Lecuit, T., Samanta, R. and Wieschaus, E. (2002). slam encodes a developmental regulator of polarized membrane growth during cleavage of the Drosophila embryo. *Dev. Cell* **2**, 425-436.
Llimargas, M., Strigini, M., Katidou, M., Karagogeos, D. and Casanova, J. (2004). Lachesin is a component of a septate junction-based mechanism that controls tube size and epithelial integrity in the Drosophila tracheal system. *Development* **131**, 181-190.
Lum, L., Yao, S., Mozer, B., Rovescalli, A., Von Kessler, D., Nirenberg, M. and Beachy, P. A. (2003). Identification of Hedgehog pathway components by RNAi in Drosophila cultured cells. *Science* **299**, 2039-2045.
Malone, C. J., Misner, L., Le Bot, N., Tsai, M. C., Campbell, J. M., Ahringer, J. and White, J. G. (2003). The C. elegans hook protein, ZYG-12, mediates the essential attachment between the centrosome and nucleus. *Cell* **115**, 825-836.
Merrill, P. T., Sweeton, D. and Wieschaus, E. (1988). Requirements for autosomal gene activity during precellular stages of Drosophila melanogaster. *Development* **104**, 495-509.
Mosley-Bishop, K. L., Li, Q., Patterson, L. and Fischer, J. A. (1999). Molecular analysis of the klarsicht gene and its role in nuclear migration within differentiating cells of the Drosophila eye. *Curr. Biol.* **9**, 1211-1220.
Mounkes, L., Kozlov, S., Burke, B. and Stewart, C. L. (2003). The laminopathies: nuclear structure meets disease. *Curr. Opin. Genet. Dev.* **13**, 223-230.
Muller, H. A. and Wieschaus, E. (1996). armadillo, bazooka, and stardust are critical for early stages in formation of the zonula adherens and maintenance of the polarized blastoderm epithelium in Drosophila. *J. Cell Biol.* **134**, 149-163.
Muller, H. A. and Bossinger, O. (2003). Molecular networks controlling epithelial cell polarity in development. *Mech. Dev.* **120**, 1231-1256.
Pankratz, M. J. and Jackle, H. (1993). Blastoderm segmentation. In *The Development of Drosophila melanogaster vol. 1* (ed. M. Bate and A. Martinez-Arias), pp. 467-516. New York: Cold Spring Harbor Laboratories Press.
Papoulas, O., Hays, T. S. and Sisson, J. C. (2005). The golgin Lava lamp mediates dynein-based Golgi movements during Drosophila cellularization. *Nat. Cell Biol.* **7**, 612-618.
Pelissier, A., Chauvin, J. P. and Lecuit, T. (2003). Trafficking through Rab11 endosomes is required for cellularization during Drosophila embryogenesis. *Curr. Biol.* **13**, 1848-1857.
Postner, M. A. and Wieschaus, E. F. (1994). The nullo protein is a component of the actin-myosin network that mediates cellularization in Drosophila melanogaster embryos. *J. Cell Sci.* **107**, 1863-1873.
Robinson, J. T., Wojcik, E. J., Sanders, M. A., McGrail, M. and Hays, T. S. (1999). Cytoplasmic dynein is required for the nuclear attachment and migration of centrosomes during mitosis in Drosophila. *J. Cell Biol.* **146**, 597-608.
Rose, L. S. and Wieschaus, E. (1992). The Drosophila cellularization gene nullo produces a blastoderm-specific transcript whose levels respond to the nucleocytoplasmic ratio. *Genes Dev.* **6**, 1255-1268.
Schejter, E. D. and Wieschaus, E. (1993a). bottleneck acts as a regulator of the microfilament network governing cellularization of the Drosophila embryo. *Cell* **75**, 373-385.
Schejter, E. D. and Wieschaus, E. (1993b). Functional elements of the cytoskeleton in the early Drosophila embryo. *Annu. Rev. Cell Biol.* **9**, 67-99.
Schweisguth, F., Lepesant, J. A. and Vincent, A. (1990). The serendipity alpha gene encodes a membrane-associated protein required for the cellularization of the Drosophila embryo. *Genes Dev.* **4**, 922-931.
Serano, J. and Rubin, G. M. (2003). The Drosophila synaptotagmin-like protein bitesize is required for growth and has mRNA localization sequences within its open reading frame. *Proc. Natl. Acad. Sci. USA* **100**, 13368-13373.
Sisson, J. C., Field, C., Ventura, R., Royou, A. and Sullivan, W. (2000). Lava lamp, a novel peripheral golgi protein, is required for Drosophila melanogaster cellularization. *J. Cell Biol.* **151**, 905-918.
Sonnichsen, B., Koski, L. B., Walsh, A., Marschall, P., Neumann, B., Brehm, M., Alleaume, A. M., Artelt, J., Bettencourt, P., Cassin, E. et al. (2005). Full-genome RNAi profiling of early embryogenesis in Caenorhabditis elegans. *Nature* **434**, 462-469.
Starr, D. A., Hermann, G. J., Malone, C. J., Fixsen, W., Priess, J. R., Horvitz, H. R. and Han, M. (2001). unc-83 encodes a novel component of the nuclear envelope and is essential for proper nuclear migration. *Development* **128**, 5039-5050.
Stathopoulos, A., Van Drenth, M., Erives, A., Markstein, M. and Levine, M. (2002). Whole-genome analysis of dorsal-ventral patterning in the Drosophila embryo. *Cell* **111**, 687-701.
Stein, J. A., Broihier, H. T., Moore, L. A. and Lehmann, R. (2002). Slow as molasses is required for polarized membrane growth and germ cell migration in Drosophila. *Development* **129**, 3925-3934.
Swan, A., Nguyen, T. and Suter, B. (1999). Drosophila Lissencephaly-1 functions with Bic-D and dynein in oocyte determination and nuclear positioning. *Nat. Cell. Biol.* **1**, 444-449.
Tepass, U., Gruszynski-DeFeo, E., Haag, T. A., Omatyar, L., Torok, T. and Hartenstein, V. (1996). shotgun encodes Drosophila E-cadherin and is preferentially required during cell rearrangement in the neurectoderm and other morphogenetically active epithelia. *Genes Dev.* **10**, 672-685.
Uemura, T., Oda, H., Kraut, R., Hayashi, S., Kotaoka, Y. and Takeichi, M. (1996). Zygotic Drosophila E-cadherin expression is required for processes of dynamic epithelial cell rearrangement in the Drosophila embryo. *Genes Dev.* **10**, 659-671.
Welte, M. A., Gross, S. P., Postner, M., Block, S. M. and Wieschaus, E. F. (1998). Developmental regulation of vesicle transport in Drosophila embryos: forces and kinetics. *Cell* **92**, 547-557.
White, K. P., Rifkin, S. A., Hurban, P. and Hogness, D. S. (1999). Microarray analysis of Drosophila development during metamorphosis. *Science* **286**, 2179-2184.
Wieschaus, E. and Sweeton, D. (1988). Requirements for X-linked zygotic gene activity during cellularization of early Drosophila embryos. *Development* **104**, 483-493.
Zhang, F. L. and Casey, P. J. (1996). Protein prenylation: molecular mechanisms and functional consequences. *Annu. Rev. Biochem.* **65**, 241-269.